

Supplementary Information

Boyang Qin^{1,2}, Ranjiangshang Ran¹, Paul F. Salipante³, Steven D. Hudson³, and Paulo E. Arratia¹

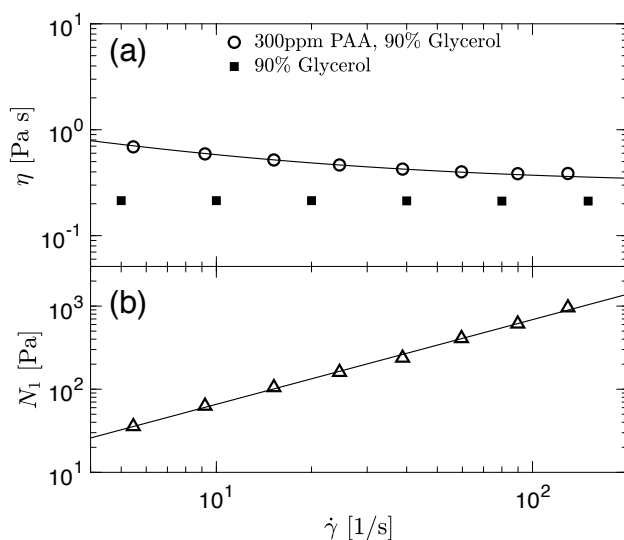
¹Department of Mechanical Engineering & Applied Mechanics, University of Pennsylvania, Philadelphia, 19104, USA

²Department of Mechanical and Aerospace Engineering, Princeton University, Princeton, 08544, USA

³Polymers & Complex Fluids Group, National Institute of Standards and Technology, Gaithersburg, 20899, USA

1 Fluid Rheology

Both viscoelastic and Newtonian fluids are used in the experiments. Viscoelastic fluids are prepared by adding small amounts of the flexible polymer polyacrylamide (PAA, 18×10^6 MW) to a 90% by weight glycerol aqueous solution, which is a viscous Newtonian solvent of viscosity 0.21 Pa·s. This solvent is used as Newtonian control group. The PAA polymer overlap concentration (c^*) is approximately 350 ppm and the viscoelastic solution is 300 ppm ($c/c^*=0.86$) [1]. Under the shear rates used in the experiments, the viscosity of the solution is weakly dependent on the shear rate.

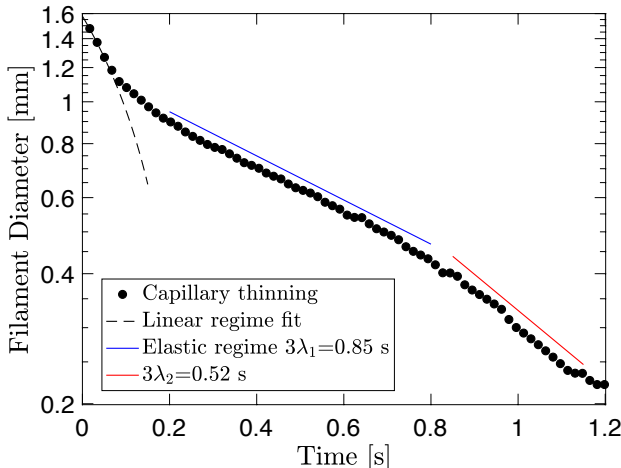


SI Fig. 1 – Steady shear rheological measurements. (a) Shear viscosity $\eta(\dot{\gamma})$ and (b) normal stress difference $N_1(\dot{\gamma})$ of viscoelastic fluids as a function of shear rate ($\dot{\gamma}$), measured using a strain-controlled cone-plate rheometer at an ambient temperature of 21 °C.

We use a strain-controlled cone-plate rheometer (Bohlin, Malvern) at 21°C to characterize the fluids. Shear viscosity data shows that the viscoelastic fluid has nearly constant viscosity ~ 0.3 Pa·s for shear rates ($\dot{\gamma}$) from $5 s^{-1}$ to $100 s^{-1}$. This range of shear rates is common in our experiments. Fitting the data to a simple

power law model we obtain an exponent of 0.81 which means weak shear-thinning viscosity behavior (SI Fig. 1a). The first normal stress difference N_1 , due to elastic stresses in the polymeric fluid is also measured in the cone-plate geometry (SI Fig. 1b).

To quantify the dominant *extensional* relaxation time of the fluid, we employ an in-house filament thinning method. At room temperature 21°C, a free hanging drop of polymeric fluid is allowed to extend under the influence of gravity and the diameter of the midsection of the filament is tracked over time, as shown in SI Fig. 2. After the initial linear regime, the relaxation time is found to be $\lambda \approx 2.3$ sec in the elastic regime, before finite extension takes place.



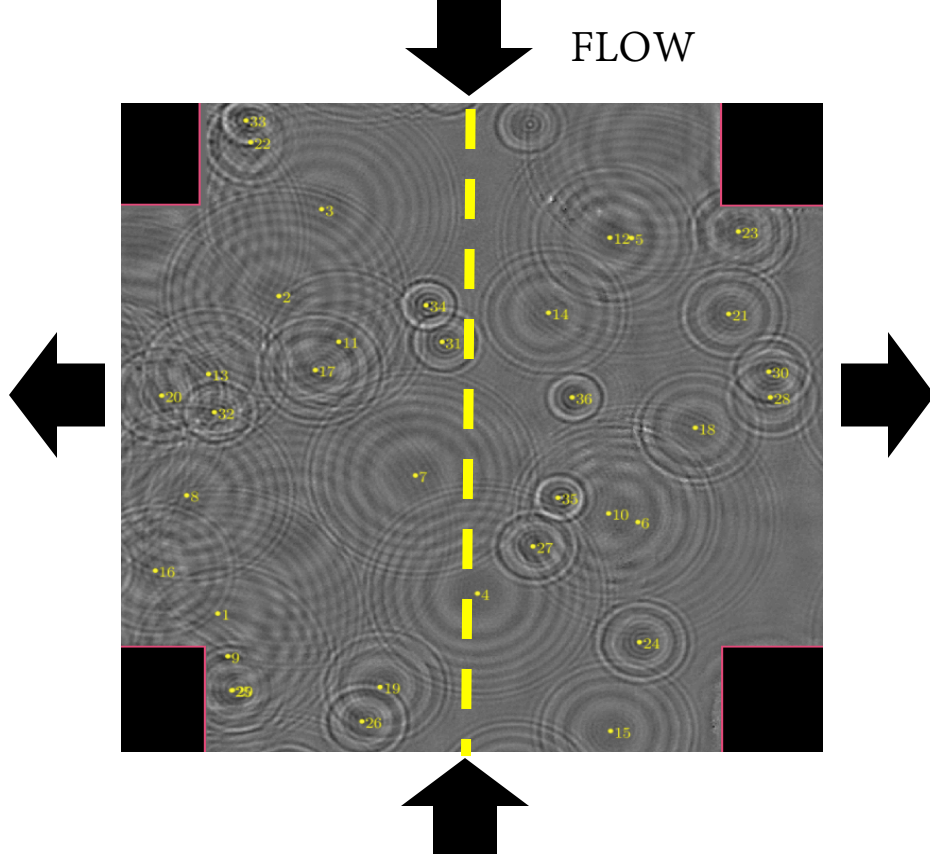
SI Fig. 2 – Filament thinning experiment measuring extensional relaxation time of the polymeric fluid.

2 Pressure Measurement Scheme

To obtain pressure drop measurements in the microchannel, we use pressure sensors (Honeywell TBPDANS compensated/unamplified series) of different ranges (1-15psi). The typical time response is 1ms and the measurement accuracy is 0.15% of the full scale. These sensors are placed in a pitot style arrangement. At specified location on the channel, we create a short side branch to the main channel that is fully sealed by the glass. At the end of the side branch, a dead-end chamber is formed by inserting the pressure taps. This ensures that no volume flow can enter this branch in steady state.

3 Holographic Particle Tracking

In order to obtain 3-dimensional Lagrangian particle trajectories at high spatial and temporal resolution, we use holographic particle tracking scheme adapted from [2, 3]. The flow is seeded with tracers (1 μm diam) which are imaged using a microscope and a CMOS camera (6000 fps). Under a coherent light source (DPSS 532nm Laser), tracer particles induce a light scattering field which is projected onto the imaging plane. This scattering image, after application of background subtract algorithm, is shown in SI Fig. 3 where identified particles are indexed in the order of their separation from the image plane. The out-of-plane (z) positions of tracer particles are reconstructed by finding the local maxima of the 3-d convolution between the scattering image and the Rayleigh-Sommerfeld kernel. Standard particle tracking are then used to connect the centroids to form Lagrangian particle trajectories. The uncertainty of estimated particle centroid can be estimated by the standard deviation in each (x, y, z) components and is around 30nm for the in-plane (x, y) components and 0.6 μm for the out-of-plane z , at experimental seeding density (10^{-5} weight fraction). Measurement window of the trajectories is located in a cubic window centered around the cross-channel center.

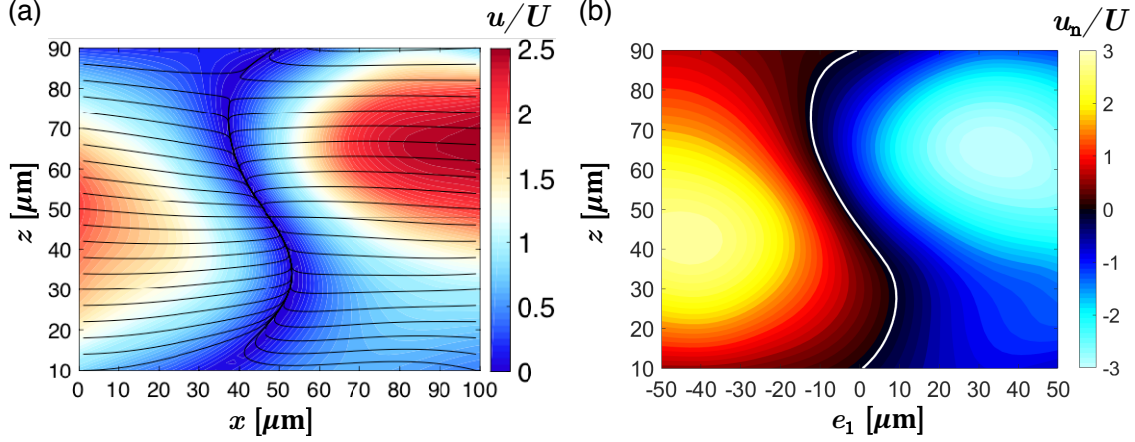


SI Fig. 3 – Particle holograms used in the holographic particle tracking velocimetry. Particles near the imaging plane ($5 \mu\text{m}$ below bottom wall) induce rings with smaller radius.

4 Separatrix Measurements and Mode Computation

The mode shape and strength is calculated directly from 3-d velocimetry data. For each flow rate, the separatrix between the inflow streams (along x) are defined as the manifold where u_x is zero. Once the manifold is obtained, its intersection with the x - z plane is isolated and used to represent the separatrix during mode analysis. The mode amplitudes are computed using around 10 separate velocimetry trials (measurements), each lasting 12 sec. Depending on the flow rate, around 0.1 sec worth of velocimetry data is used to generate each separatrix trials to give a total of ~ 500 samples. The amplitude of each buckling mode is computed by taking a dot product between the separatrix and the mode waveform.

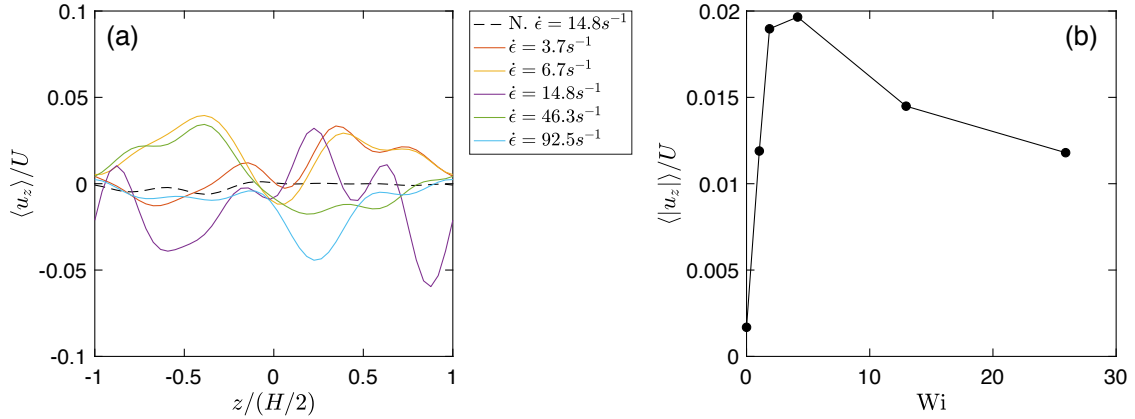
To measure the profile of the separatrix, we have chosen a fix vertical (x - z) plane along the center of the cross-channel. This approach eliminates the need to constantly change perspective and observation window and ensures consistency between measurements, in contrast to an observation plane that is moving in space. Moreover, over many observation samples, the form of the separatrix along the x - z plane is similar to that along a cut plane that is 45° to the inflow x direction for example, as is shown in SI Fig. 4.



SI Fig. 4 – Comparison of separatrix waveforms ($\dot{\epsilon} = 10 \text{ s}^{-1}$, $Wi = 3$) sectioned at different observation planes for (a) the x - z vertical plane passing through the cross-channel center and (b) the e_1 - z plane that is at 45° relative to the plane in (a). The black curve in (a) and the white curve in (b) denote the respective separatrix waveforms. Here u is the local velocity magnitude and u_n is the local velocity magnitude normal to the observation plane. Streamlines in (b) are excluded for clarity.

5 Vertical Velocity Component along the Channel Vertical Centerline

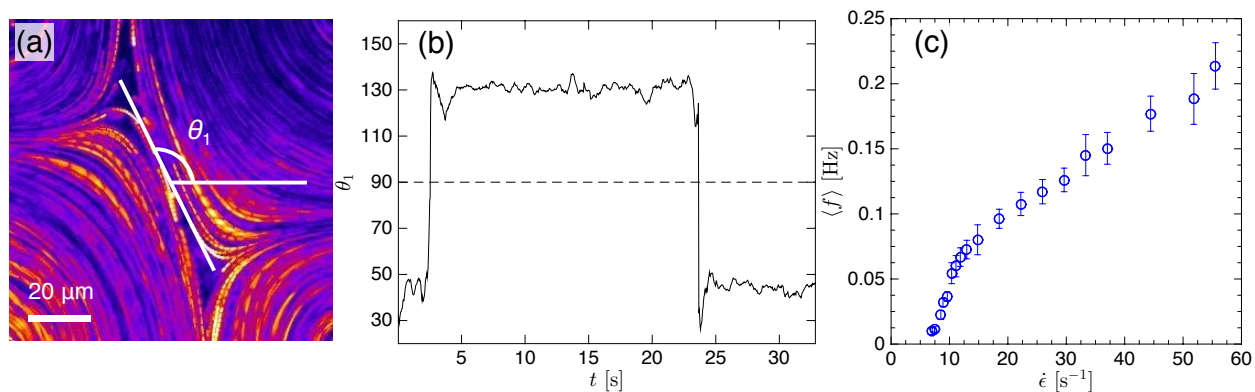
The vertical velocity profile along the center of the cross-channel is shown in SI Fig. 5.



SI Fig. 5 – (a) Time-averaged tertiary velocity component u_z normalized by mean flow velocity U along a vertical cutline at the center of the cross-channel. Time window used for averaging is 3 sec. (b) The mean absolute value of the tertiary velocity component u_z for the flow rates shown in (a).

6 Switching Frequency of 2D Bistable Instability

To quantify the 2D bistable flow switching, we measure the characteristic frequencies of the 2D by conventional microscopy image taken at the $x - y$ mid-plane of the cross-channel for extended periods (1 hour). SI Fig. 6. show that the frequency of the 2D switching vanishes near the critical strain rate.



SI Fig. 6 – (a) Particle streaks (0.1 sec image exposure) of $1 \mu\text{m}$ fluorescent particles imaged in the $x - y$ mid plane of the cross-channel, showing the well-known unsteady 2D asymmetric flow. The flow orientation is defined by the eigenvector of the image moment matrix of the particle streak image, as shown by θ_1 . (b) Flow switching events as captured by the time change in θ_1 . (c) Average flow switching frequency obtained by time course of θ_1 for various flow extensional rates (each data point represents about 1 h of continuous time series measurements). The flow switching period diverges near the critical extensional rate 4 s^{-1} .

References

- [1] Pelletier, E., Viebke, C., Meadows, J. & Williams, P.A. *Langmuir* 19, 559-565 (2003).
- [2] Cheong F. C., Krishnatreya B. J., & Grier D. G., *Opt. Express* 18, 13563 (2010).
- [3] Salipante, P. F., Little C. A., & Hudson, S. D., *Phys. Rev. Fluids* 2, 033302 (2017).